Loss of ATRX leads to chromosome cohesion and congression defects

Kieran Ritchie,[1,2] Claudia Seah,[1,2] Jana Moulin,[1,2] Christian Isaac,[1,2] Frederick Dick,[1,2,3,4] and Nathalie G. Bérubé[1,2,3]

[1]Department of Paediatrics and [2]Department of Biochemistry, University of Western Ontario, London, Canada N6A 4L6
[3]Children's Health Research Institute, London, Canada N6C 2V5
[4]London Regional Cancer Centre, London, Canada N6A 4L6

α Thalassemia/mental retardation X linked (ATRX) is a switch/sucrose nonfermenting-type ATPase localized at pericentromeric heterochromatin in mouse and human cells. Human *ATRX* mutations give rise to mental retardation syndromes characterized by developmental delay, facial dysmorphisms, cognitive deficits, and microcephaly and the loss of ATRX in the mouse brain leads to reduced cortical size. We find that ATRX is required for normal mitotic progression in human cultured cells and in neuroprogenitors. Using live cell imaging, we show that the transition from prometaphase to metaphase is prolonged in ATRX-depleted cells and is accompanied by defective sister chromatid cohesion and congression at the metaphase plate. We also demonstrate that loss of ATRX in the embryonic mouse brain induces mitotic defects in neuroprogenitors in vivo with evidence of abnormal chromosome congression and segregation. These findings reveal that ATRX contributes to chromosome dynamics during mitosis and provide a possible cellular explanation for reduced cortical size and abnormal brain development associated with ATRX deficiency.

Introduction

α Thalassemia/mental retardation X linked (ATRX) is a chromatin remodeling enzyme implicated in early development of several organs, particularly the central nervous system. The ATRX protein contains conserved domains that suggest a role in the epigenetic regulation of chromatin structure and function, including a plant homeodomain-like zinc finger domain shared with de novo methyltransferases (DNMT3A/B and 3L) and a switch/sucrose nonfermenting family ATPase domain. ATRX has the ability to remodel chromatin and displays ATP-dependent translocase activity (Xue et al., 2003). It is highly enriched at pericentromeric heterochromatin (PCH) in mouse and human cells (McDowell et al., 1999) and associates directly with the chromoshadow domain (CSD) of heterochromatin protein 1α (HP1α; Lechner et al., 2005). It is also targeted to promyelocytic leukemia nuclear bodies by the C-terminal portion of the protein (Berube et al., 2007). *Atrx* loss of function in the mouse starting at cell stage 8 to 16 is embryonically lethal (Garrick et al., 2006) and conditional ablation of the full-length ATRX isoform in the mouse forebrain results in decreased cortical size at birth (Berube et al., 2005). Although ATRX has been proposed to regulate gene transcription, the protein appears to be hyperphosphorylated and highly enriched at condensed chromosomes during mitosis in human cells, which suggests an additional function during this stage of the cell cycle (Berube et al., 2000).

The faithful segregation of chromosomes during mitosis requires the physical linkage of sister chromatids from S phase until the onset of anaphase. The ring-shaped cohesin multiprotein complex is required for the maintenance of sister chromatid cohesion and plays a role in the proper separation and segregation of sisters during anaphase (Hirano, 2005). Cohesin at the chromosomal arms is released during prophase by the polo and aurora B kinases and the chromatin protein wings apart–like (Sumara et al., 2002; Gandhi et al., 2006; Kueng et al., 2006). Cohesion at PCH is protected by the Shugoshin family of proteins and prohibitin 2, and consequently persists until all the chromosomes are bioriented at the metaphase plate (McGuinness et al., 2005; Kitajima et al., 2006; Takata et al., 2007). Only then is the spindle checkpoint satisfied, resulting in the activation of the anaphase-promoting complex/cyclosome and subsequent cohesin cleavage by the thiol protease separase.

Correspondence to N.G. Bérubé: nberube@uwo.ca

Abbreviations used in this paper: ANOVA, analysis of variance; ATRX, α thalassemia/mental retardation X linked; CdLS, Cornelia de Lange syndrome; CENP, centromere-associated protein; CREST, calcinosis, Raynaud's phenomenon, esophageal dismotility, sclerodactyly, and telangiectasia; CSD, chromoshadow domain; E, embryonic day; HG, HeLa-H2B-GFP; HP1, heterochromatin-binding protein 1; NIPBL, nipped-B–like; PCH, pericentromeric heterochromatin; Q-RT-PCR, quantitative RT-PCR.

The online version of this paper contains supplemental material.

The Journal of Cell Biology, Vol. 180, No. 2, January 28, 2008 315–324
http://www.jcb.org/cgi/doi/10.1083/jcb.200706083

Stable loading of cohesin onto chromatin before DNA replication is mediated by the Scc2-Scc4 heterodimer in yeast (Ciosk et al., 2000; Watrin et al., 2006). Human Scc2, known as nipped-B–like (*NIPBL* [delangin]), mediates cohesin transfer onto chromatin during S phase and, like ATRX, associates with the CSD of HP1α (Lechner et al., 2005). Chromatin remodeling proteins have been implicated in chromosome cohesion. The Sth1 subunit of the yeast RSC chromatin remodeling complex has been shown to participate in cohesin loading on chromosomal arms but not at the centromere (Baetz et al., 2004; Huang et al., 2004). In human cells, the SNF2h/ISWI chromatin remodeling protein, a component of several remodeling complexes, was shown to participate in cohesin recruitment to specific sites on chromosome arms (Hakimi et al., 2002).

ATRX mutations in humans cause mental retardation and microcephaly (Gibbons et al., 1995; Picketts et al., 1996). Given that *Atrx* loss of function in the mouse forebrain results in reduced cortical mass (Berube et al., 2005) and that the protein becomes hyperphosphorylated at the onset of mitosis (Berube et al., 2000), we postulated that ATRX could have specific functions during mitosis. We now provide evidence that the switch/sucrose nonfermenting-like chromatin remodeling protein ATRX is required for normal chromosome congression, cohesion, and segregation in human cultured cells. Loss of ATRX in neuronal progenitors by Cre/loxP recombination in vivo also resulted in abnormal chromosome segregation, as indicated by the high incidence of micronuclei and dispersed chromosomes. Mitotic dysfunction could induce cell death in the developing brain and/or cause a reduction in symmetric cell divisions, therefore reducing the progenitor pool. Either of these scenarios or a combination thereof would be predicted to reduce cortical size at birth.

Results

ATRX-depleted HeLa cells exhibit unusual nuclear morphology and DNA bridging

The *ATRX* gene yields two major protein isoforms: a full-length 280-kD protein and a truncated form, ATRXt, of 180 kD (Garrick et al., 2004). Both ATRX protein isoforms exhibit exclusive nuclear localization and are highly enriched at PCH (Fig. 1, A and C). We induced transient ATRX depletion in HeLa cells by transfecting siRNAs. Cells were treated with two siRNA duplexes, siATRX1 and siATRX2, each designed to simultaneously silence the full-length and truncated ATRX proteins. Both duplexes caused substantial silencing of ATRX isoforms as assessed by immunostaining (Fig. S1 A, available at http://www.jcb.org/cgi/content/full/jcb.200706083/DC1), and this was confirmed by quantitative RT-PCR (Q-RT-PCR; Fig. S1 B) and Western blot analysis (Fig. 1 B). Coimmunofluorescence staining of centromeres using the calcinosis, Raynaud's phenomenon, esophageal dismotility, sclerodactyly, and telangiectasia (CREST) antibody demonstrated that only minimal amounts of ATRX protein are detectable at PCH in siRNA-treated cells (Fig. 1 C). We observed that the nuclei of depleted cells appeared lobulated and that the cells showed evidence of intranuclear DNA bridges and poorly resolved chromatin masses during interphase (Fig. 1 D). We scored the number of abnormal nuclei at 48, 72, and 96 h after transfection and found an increased incidence of lobulated nuclei and intranuclear bridges (Fig. 1 E). Such abnormalities can be indicative of mitotic defects and prompted us to further investigate the function of ATRX in mitosis.

Prolonged prometaphase-to-metaphase transition upon down-regulation of ATRX

To investigate the kinetics of mitotic progression, we assessed the outcome of both transient and stable depletion of ATRX in HeLa cells that express histone H2B fused to GFP (HeLa-H2B-GFP [HG]). Stable clones were difficult to expand, which suggests that reduced ATRX expression imparts negative effects on cell division, proliferation, or viability. A negative impact on cell division was previously reported upon conditional ablation of the full-length ATRX protein in embryonic stem cells, although the cause was not determined (Garrick et al., 2006). We chose two stable cell lines for our analysis, designated shATRX1 and shATRX2, each expressing a short hairpin RNA that targets a distinct sequence within the *ATRX* transcript. Both stable clones expressed substantially reduced levels of *ATRX* RNA and protein as determined by Q-RT-PCR and Western blot analysis (Fig. 2 A).

Time-lapse videomicroscopy was used to evaluate the outcome of both transient and stable ATRX silencing. We generated videos of live cells (10 h) and from these measured the time required to complete each stage of mitosis (stable clone, $n = 50$; transient depletion, $n \geq 120$). This analysis revealed that ATRX-depleted cells took longer than control cells to undergo mitosis (Fig. S2, available at http://www.jcb.org/cgi/content/full/jcb.200706083/DC1) because of an extended transition from prometaphase to fully aligned metaphase (Fig. 2 B; $P < 0.001$). The delays in prometaphase were underestimated because a subset of mitotic cells that were arrested at prometaphase or metaphase for the total duration of the observation period (10 h) were not included in this analysis. These chronically arrested prometaphase cells often became nonadherent and/or died, as indicated by membrane blebbing and highly condensed chromatin (Video 1). Collectively, these results show that ATRX is required for the normal transition from prometaphase to metaphase during mitosis.

ATRX depletion affects chromosome congression

The mitotic delay in ATRX-depleted cells occurred primarily between prometaphase and metaphase, a time when condensed chromosomes are congressing toward the metaphase plate. We noticed that metaphase plates in transiently depleted cells and in the shATRX1 and shATRX2 stable cell lines were often characterized by misaligned chromosomes or chromosomes that remained randomly distributed over the bipolar microtubule spindle (Fig. 2 C and Video 2, available at http://www.jcb.org/cgi/content/full/jcb.200706083/DC1), which suggests that the prometaphase-to-metaphase delay might be caused by impaired chromosome congression to the spindle equator. To evaluate the extent of this defect, we scored the number of metaphasic cells with misaligned chromosomes in control and ATRX-depleted live cell cultures. A greater proportion of metaphase plates had

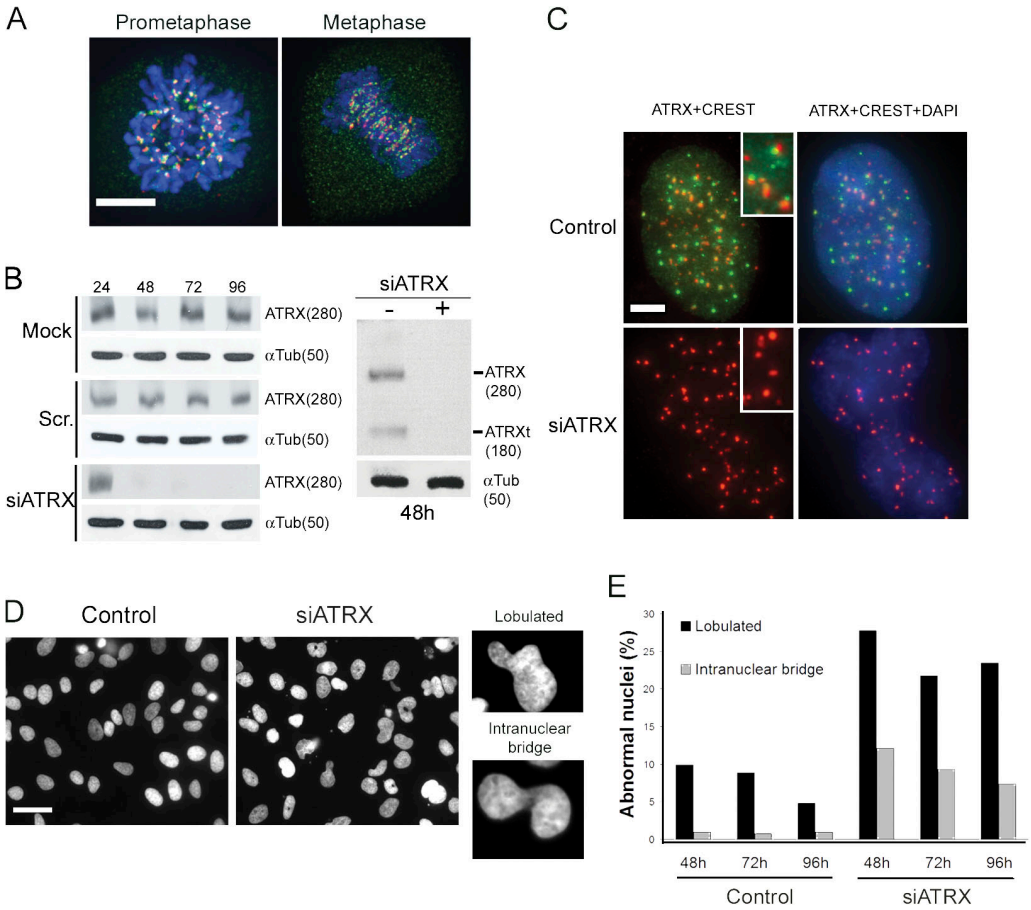

Figure 1. **Transient ATRX depletion in HeLa cells induces abnormal nuclear morphology.** (A) Immunofluorescence detection of ATRX (green) and the kinetochore marker CREST (red) on prometaphase and metaphase chromosomes. (B) Western blot analysis of HeLa cells transiently transfected with siATRX 19-mer duplexes demonstrate ATRX protein depletion starting at 48 h and up to 96 h after transfection. ATRX protein levels remained constant upon mock transfection and in cells transfected with a control siATRX scrambled sequence duplex (left). Both ATRX isoforms were effectively silenced by 48 h after transfection (right). α-Tubulin protein expression (αTub) was used as a control in all experiments. Numbers on top of the blot indicate hours after transfection and numbers in parenthesis indicate the molecular mass in kD. (C) Costaining of kinetochores and ATRX with the CREST and 39f antibodies, respectively, reveals loss of ATRX protein at PCH in siRNA-treated cells. (D) Cells stained with DAPI show abnormal nuclear morphology in ATRX-depleted cells compared with control cells. Common defects include lobulated nuclei and intranuclear DNA bridges (right). (E) The number of nuclei displaying abnormalities was quantified at 48, 72, and 96 h after siRNA treatment (n > 1,000 nuclei at each time point). Bars: (A and C) 5 μm; (D) 20 μm.

misaligned chromosomes in the shATRX1- and shATRX2-depleted clones compared with controls (Fig. 2, C and E). In addition, we followed stably (shATRX1, $n = 100$) and transiently (siATRX, $n \geq 120$) depleted mitotic cells by videomicroscopy over a 10-h period and observed an approximately threefold (stable depletion) and fourfold (transient depletion) increase in the number of cells displaying congression defects in ATRX-depleted cells compared with control cells during that time period (Fig. 2 D). In addition, metaphasic cells often appeared less condensed in ATRX-depleted cells and were sometimes observed to undergo decondensation/recondensation before anaphase onset by live imaging (Fig. 2 E, middle; and Video 3). We further confirmed the general decondensed appearance of ATRX-depleted metaphasic chromosomes by staining chromosome spreads with DAPI. The frequency of spreads with a staining pattern indicative of more decondensed chromatin (wider chromosomes) was higher in cells transiently depleted of ATRX using siATRX1 and siATRX2 duplexes (Fig. 2 F) than in control cells. These results demonstrate that transient as well as stable silencing of ATRX interferes with normal prometaphase-to-metaphase progression, causes impaired chromosome congression, and is sometimes accompanied by chromosome decondensation.

Sister chromatid cohesion is compromised in ATRX-depleted cells

Abnormal chromosomal congression could be caused by perturbed targeting of outer kinetochore proteins to the centromere, spindle defects, abnormal PCH, or reduced cohesion between sister chromatids. Congression defects have been reported upon depletion of the outer kinetochore proteins centromere-associated protein (CENP)-E and CENP-F (mitosin) that are essential for stable microtubule–kinetochore capture (Wood et al., 1997; Yao et al., 1997; McEwen et al., 2001; Tanudji et al., 2004; Yang et al., 2005). We examined the ability of CENP-E and CENP-F to localize to kinetochores in ATRX-depleted cells and found that both proteins localized normally at the kinetochore of metaphasic cells (Fig. 3 A). The loss of factors that control PCH structure can also cause aberrant mitosis (Melcher et al., 2000;

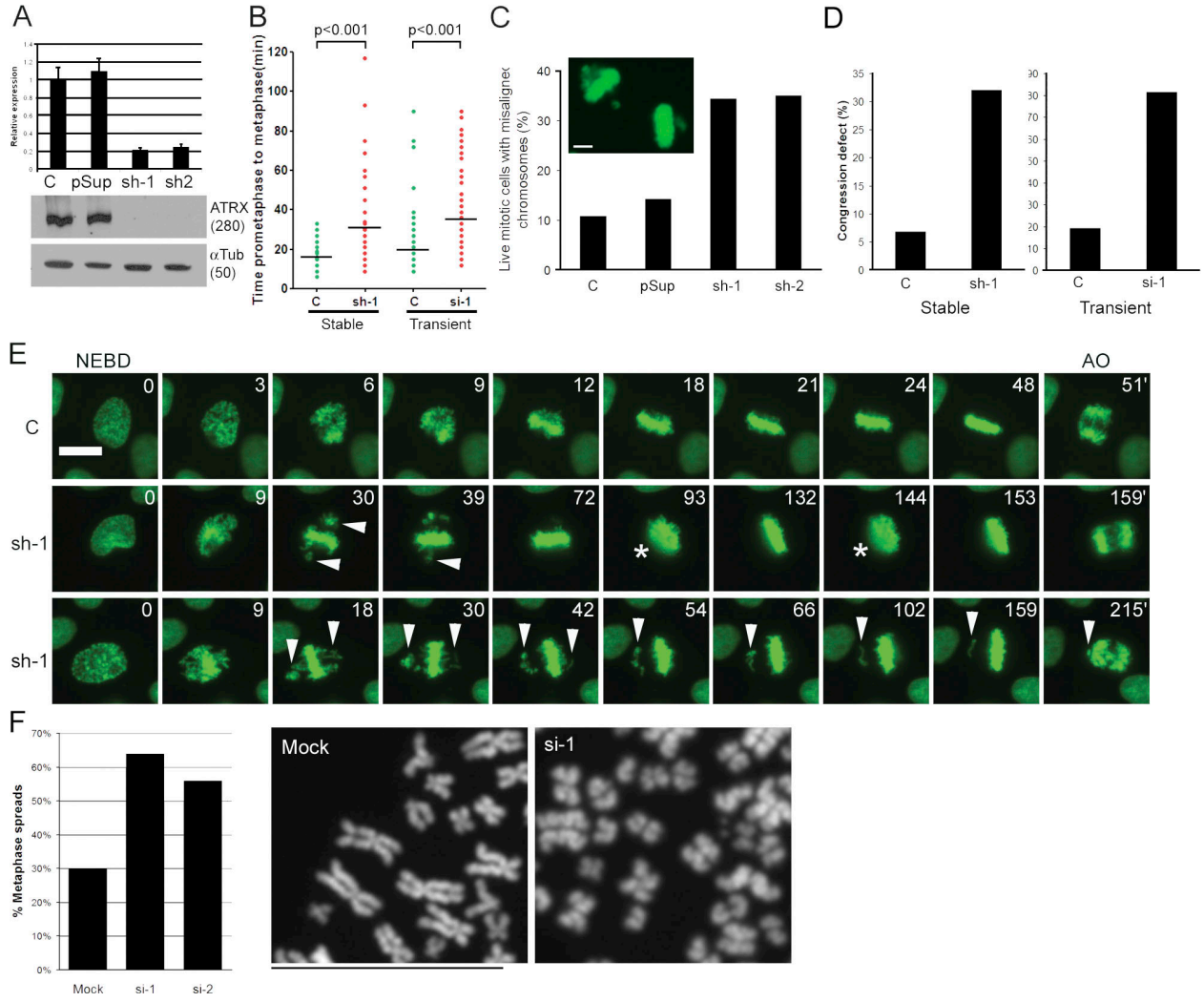

Figure 2. **Stable and transient depletion of ATRX extends the transition to metaphase and induces congression defects.** (A) HeLa-HG cells that stably express pSuper-shATRX1, pSuper-shATRX2, or pSuper (empty vector control) were generated and the level of ATRX depletion was measured by Q-RT-PCR (top) and Western blot analysis (bottom). Q-RT-PCR results were normalized to GAPDH expression and protein loading on the Western blot was controlled with α-tubulin. Error bars represent the standard deviation from triplicate samples. (B) Mitotic cells were followed in real time by videomicroscopy and the duration of prometaphase was measured for HG control and HG-shATRX1 stably depleted cells (n = 50 each) and also in transient transfections with siATRX1 (n > 120). Horizontal lines indicate the mean value of each dataset. (C) The fraction of metaphasic cells with misaligned chromosomes (inset) was evaluated in live cell cultures of HeLa-HG, HG-pSuper, HG-shATRX1, and HG-shATRX2 stable clones (n = 100 for each). (D) Live mitotic cells were followed over a 10 h period and scored for congression defects in stable (n = 50) and transient experiments (n > 120). (E) Selected panels from live cell videomicroscopy experiments of control HeLa-HG cells and ATRX-depleted cells from nuclear envelope breakdown (NEBD) to anaphase onset (AO). ATRX-depleted mitotic cells often displayed misaligned chromosomes (arrowheads) that resolved before the onset of anaphase (middle), whereas, in some cases, anaphase was initiated despite the presence of misaligned chromosomes (bottom). A subset of metaphase chromosomes underwent cycles of general decondensation and recondensation (the asterisk indicates a decondensed metaphase plate). Numbers indicate minutes after NEBD. (F) Morphological assessment of chromosome decondensation in control and transiently depleted cells. Graph depicts the percentage of metaphase spreads that display a more decondensed appearance (far right). Bars: (C) 5 μm; (E) 16 μm, (F) 20 μm.

Peters et al., 2001). Specific histone modifications that characterize PCH, including trimethylated H3K9 and H4K20 and monomethylated H3K27, were not visibly affected in ATRX-depleted cells (unpublished data). Trimethylation of Lys9 on histone H3 (H3K9me3) by the Suv39H1 methyltransferase recruits HP1α and forms a compact heterochromatic structure. HP1α in turn interacts with several chromatin factors, including NIPBL, ATRX, and chromatin assembly factor 1 (Lechner et al., 2005). However, we observed that nuclear HP1α as well as HP1β immunoreactivity were indistinguishable between transiently depleted and control cells (Fig. S3, available at http://www.jcb.org/cgi/content/full/jcb.200706083/DC1), which suggests that ATRX is not required for proper targeting of these proteins to PCH.

We next measured the distance between metaphasic sister kinetochores in ATRX-depleted cells using CREST immunostaining. Sister chromatid interkinetochore distances were significantly increased in both shATRX1- and shATRX2-aligned metaphases compared with control metaphases (Fig. 3 B, $P < 0.05$ by analysis of variance [ANOVA]). Increased distance between sister chromatids could reflect a more decondensed state of chromatin and perhaps fewer nucleosomes associated with

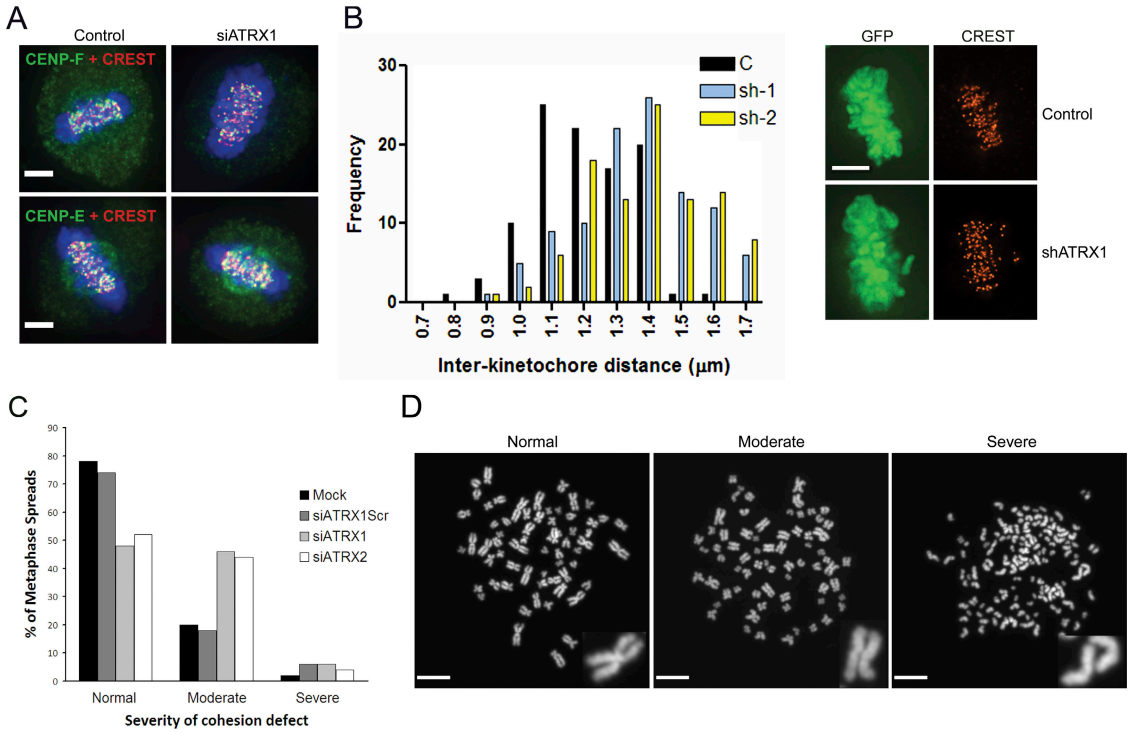

Figure 3. **Increased interkinetochore distances and reduced cohesion in ATRX-depleted cells.** (A) ATRX-depleted metaphase cells were stained for the kinetochore proteins CENP-F or CENP-E (green) in combination with CREST (red) and imaged at different z planes. Images represent an extended focus rendering of deconvoluted z stacks. (B) Control and ATRX-depleted cells were stained with anti-CREST antibody to stain kinetochores. Distances between paired kinetochores (n = 100) were measured at individual z planes and were significantly increased in shATRX1 and shATRX2 cells compared with controls ($P < 0.05$ by ANOVA). (C) Mitotic HeLa cells were transiently transfected with either siATRX-Scr control or siATRX1 and siATRX2 duplexes. After mitotic shake-off to remove any cells in mitosis, cells were treated with colcemid and chromosome spreads were stained with DAPI and scored for the percentage of chromatids displaying cohesion defects (n = 50 per treatment). Chromosomes from ATRX-depleted cells showed reduced cohesion compared with control-treated cells. (D) Microscopic images of representative chromosome spreads scored as normal (<10% cohesion defect), moderate (10–90% cohesion defect), or severe (>90% cohesion defect). Insets show representative chromosomes from each spread with normal (left), moderate (middle), and severe (right) cohesion defects. Bars: (A and B) 5 μm; (C) 20 μm.

centric chromatin. Alternatively, increased interkinetochore distances could be explained by reduced cohesion between sister chromatids. We evaluated the extent of cohesion between the chromatid pairs in DAPI-stained metaphase chromosome spreads after transient depletion using siATRX1 and siATRX2 duplexes in HeLa cells. To rule out possible effects of extended mitotic arrest (Fig. 2 B), we performed a mitotic shake-off to remove mitotic cells before colcemid treatment. As a control for nonspecific siRNA effects, cells were transfected with an siATRX1 scrambled duplex. Mitotic chromosomes from control metaphase spreads exhibited an association of the chromosome arms with a primary constriction at the centromeres, resulting in the typical "X-shaped" chromosomal morphology (Fig. 3 D, left). In contrast, after transient ATRX interference, we observed a higher proportion of chromosomes that were separated along the chromosome length with no evidence of primary centromeric constrictions, which indicates reduced centromeric cohesion (Fig. 3 C). To evaluate the extent of this defect, chromosome spreads (n = 100 per treatment) were categorized as having a normal (<10%), moderate (10–90%), or severe (>90%) loss of chromatid cohesion (Fig. 3 D). We found that ATRX-depleted cells had a higher occurrence of spreads displaying cohesion defects compared with the mock-transfected and nonspecific siRNA controls (Fig. 3 C). Severe loss of cohesion (>90% of chromosome pairs displaying loss of cohesion) was observed at low levels in both controls and depleted cells (Fig. 3, C and D), indicating that ATRX depletion results in reduced but not complete loss of sister chromatid cohesion.

ATRX depletion transiently activates the spindle checkpoint

The mitotic delay incurred by ATRX depletion prompted us to survey the status of the spindle checkpoint proteins in ATRX-depleted cells. As such, the preanaphase mitotic delay might result from continued mitotic checkpoint signaling at misaligned chromosomes. Activation of the spindle checkpoint was confirmed by staining for the checkpoint proteins BubR1 and Bub1 at misaligned chromosomes. We observed that both proteins were enriched at a subset of kinetochores in ATRX-depleted metaphases, with a strong signal at misaligned chromosomes (Fig. 4 A). We further tested the robustness of the spindle checkpoint by analyzing the fate of cells after exposure to nocodazole, a microtubule-depolymerizing agent. Nocodazole-induced mitotic arrest was robust in both control and ATRX-depleted cells, demonstrating that ATRX is not required for spindle checkpoint activation (Fig. 4 B). We next selectively destabilized nonkinetochore fibers by cold treatment. The residual intact kinetochore fibers were visualized by α-tubulin staining. We observed that

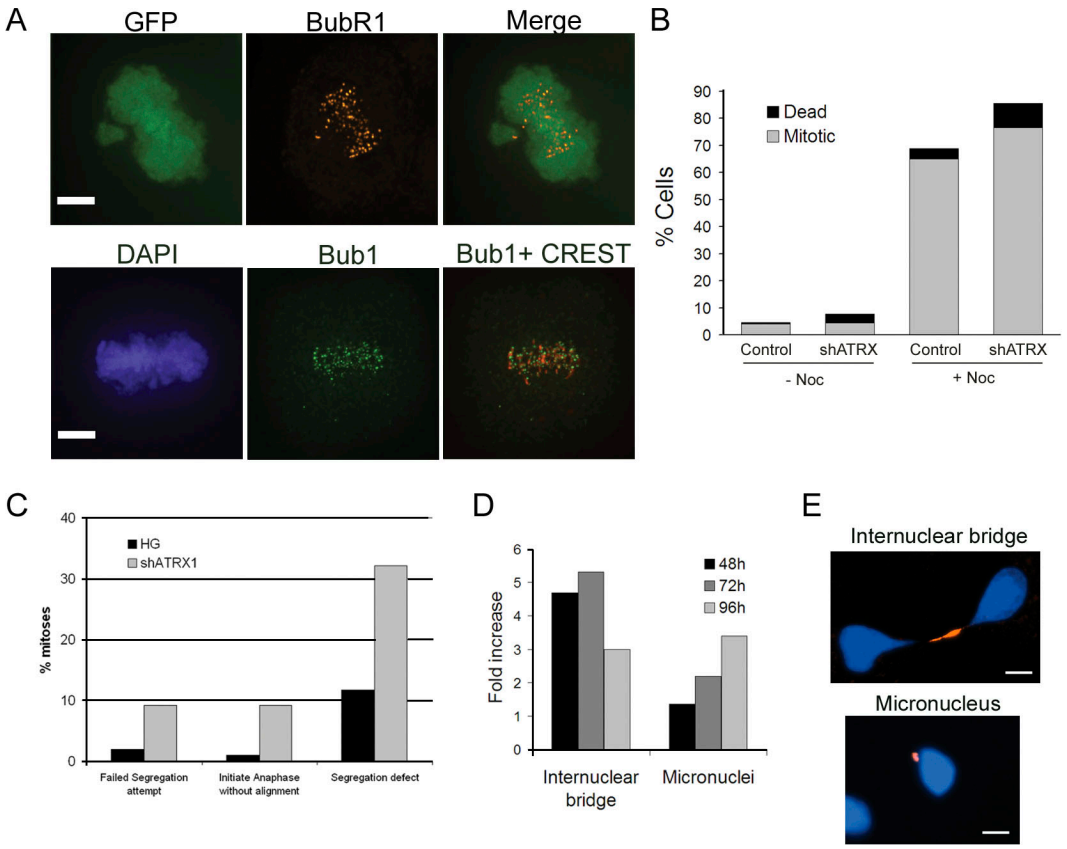

Figure 4. **Spindle checkpoint activation and aberrant chromosome segregation in ATRX-depleted cells.** (A) The spindle checkpoint protein BubR1 was detected in ATRX-depleted metaphase cells at both aligned and misaligned chromosomes (top). Another checkpoint protein, Bub1, was also found to be adjacent to the centromeres (CREST staining) in ATRX-depleted metaphase cells. (B) Mitotic index of control and ATRX-depleted cells after 16 h of nocodazole treatment. Control and ATRX-depleted cells were cultured with or without nocodazole for 16 h and live cells were photographed and scored for the percentage of mitotic rounded cells by phase imaging (n > 1,000). (C) Live cell imaging of control and ATRX-depleted mitotic cells (n = 100 for each cell line) revealed an increased number of cells that undergo repeated failed attempts at initiating anaphase, an increased number of cells that initiate anaphase without full chromosome alignment, and an increased incidence of segregation defects as indicated by the formation of chromosome DNA bridges and micronuclei. (D) The number of internuclear bridges and micronuclei indicative of chromosome missegregation were quantified at 2–4 d after transfection of the siATRX1 duplex and the fold difference between mock and depleted cells was calculated. (E) Fixed mitotic cells stained with DAPI (blue) and a phosphohistone H3S10 antibody (red) showing intranuclear DNA bridges and micronuclei in transiently depleted cells. Bars, 5 μm.

ATRX depleted cells were characterized by highly irregular arrays of kinetochore fibers (Fig. S4, available at http://www.jcb.org/cgi/content/full/jcb.200706083/DC1).

Reduced levels of ATRX induce chromosome segregation defects

Despite the activation of spindle checkpoint proteins, we observed a modest accumulation of mitotic cells in ATRX-depleted cultures by FACS analysis (Fig. S2 B), which suggests that checkpoint activation could not be maintained completely in all cells. As a result, an increased number of cells with lagging chromosomes at anaphase, telophase, and G1 (Fig. 4 D and Video 4, available at http://www.jcb.org/cgi/content/full/jcb.200706083/DC1) were observed, indicating a problem with chromosome segregation. A three- to sevenfold increase in the number of cells displaying interphase DNA bridges was observed 48–96 h after transfection with ATRX siRNA duplexes compared with control cells (Fig. 4, D and E). DNA bridges in mammalian cells produce micronuclei when the bridges resolve and reform as small membrane-bound DNA bodies (Hoffelder et al., 2004). The number of micronuclei increased 3.4-fold compared with control cells by 96 h after siRNA treatment (Fig. 4 D). Collectively, these data suggest that the spindle checkpoint control is compromised in a subset of cells, causing chromosome segregation errors characterized by lagging chromosomes, interphase DNA bridges, and the subsequent formation of micronuclei.

Defective mitosis in vivo in ATRX null neuroprogenitors

The Cre-mediated deletion of the *Atrx* gene in the developing mouse forebrain leads to a reduction in cortical and hippocampal size in newborn pups. In these mice, conditional deletion of the *Atrx* gene occurs in nearly 100% of cells in the developing forebrain starting at approximately embryonic day (E) 8.5 (Berube et al., 2005). The analysis of the mitotic defects by live cell videomicroscopy in ATRX-depleted HeLa cells provided indicators of mitotic anomalies that could potentially occur in the *Atrx* null developing mouse brain, and evidence of such abnormalities would indicate that ATRX contributes to corticogenesis in part by participating in progenitor cell mitosis. The primary progenitor cells in the developing cortex are the neuroepithelial cells in the

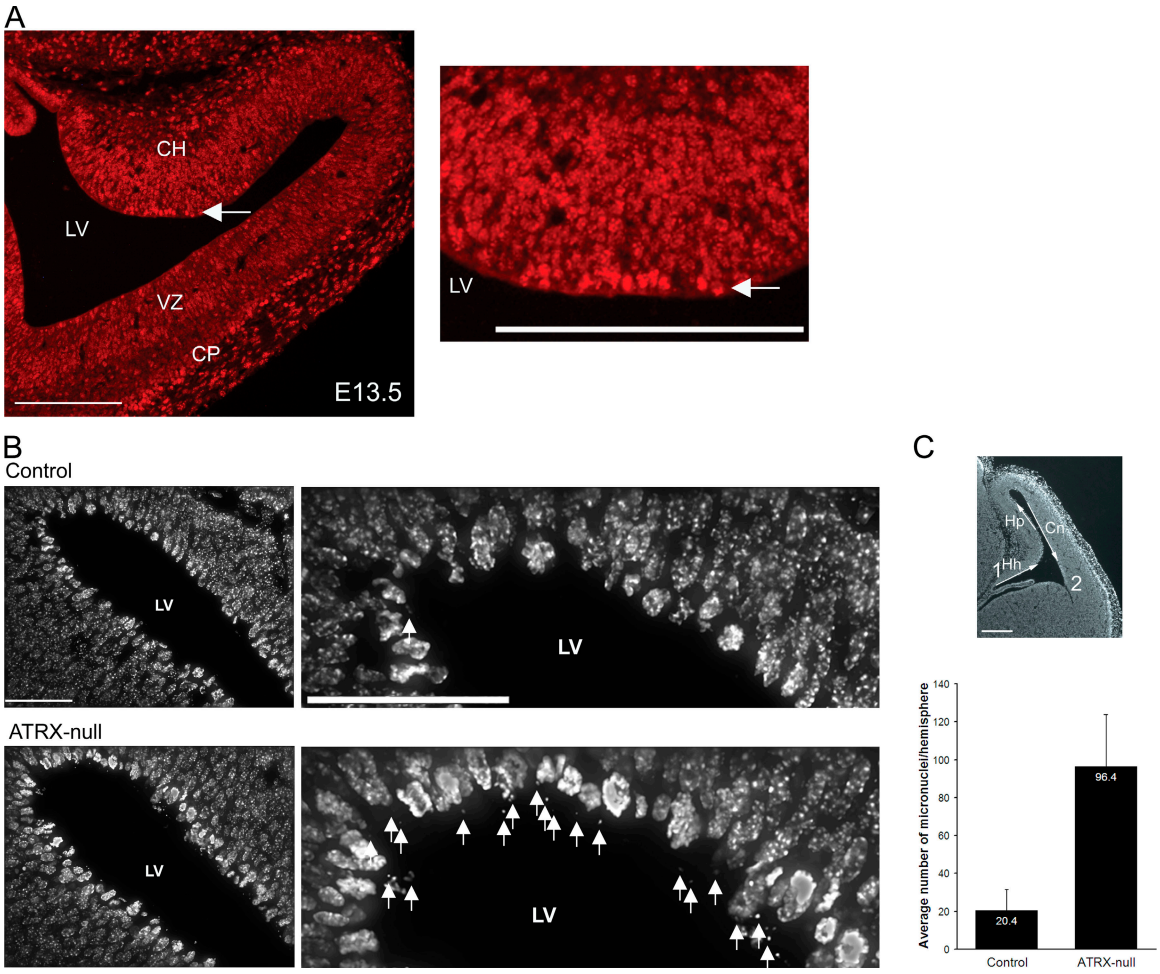

Figure 5. **ATRX association with mitotic chromosomes and evidence of mitotic defects in ATRX-deficient neuroprogenitors in vivo.** (A) ATRX staining of the cortex at E13.5. ATRX is highly expressed in all cells but is highest in the cortical hem (CH), which gives rise to hippocampal structures. ATRX is also expressed at increased levels in the differentiated neurons of developing cortical plate (CP). Mitotic cells that line the lateral ventricle are highly enriched for ATRX protein (arrows). Higher magnification of the cortical hem (right) demonstrates ATRX staining of mitotic chromosomes in cells that line the lateral ventricle (arrow). Punctate nuclear staining of ATRX in cycling cells of the ventricular zone (VZ) is characteristic of ATRX localization at PCH. (B) Cryosections obtained from control and ATRX null telencephalon were stained with DAPI to visualize mitotic chromosomes lining the lateral ventricle (LV) at E13.5. An increased incidence of micronuclei or dispersed chromosomes was detected in the vicinity of the mitotic layer (arrows) in the ATRX null embryonic brain. (C) The mean number of micronuclei or dispersed chromosomes were scored in the mitotic layer from point 1 to 2 as indicated by the white arrows (top) and are represented in the graph below (n = 4 for each control and ATRX null brain; $P < 0.0001$ by nonpaired t test). Error bars represent the standard deviation of counts from a total of 24 cortical hemisphere from a total of four brains. Cn, cortical neuroepithelium; Hh, hippocampal hem; Hp, hippocampal primordium. Bars: (A) 100 μm; (B) 40 μm; (C) 200 μm.

proliferative ventricular zone. Because of the fact that cells undergo cyclical migration within the ventricular zone, mitotic progenitors are always localized at the edge of the ventricular zone facing the lateral ventricle. Cortical sections from normal embryos at E13.5 were first examined for the pattern of ATRX protein expression and localization. ATRX immunoreactivity was indeed enriched at condensed chromatin of mitotic neuroprogenitors lining the lateral ventricle, which is consistent with a mitotic function (Fig. 5 A, arrows). ATRX was also expressed in cycling cortical progenitors in a punctate nuclear pattern characteristic of PCH in mouse cells and in differentiated neurons, as has been found previously (McDowell et al., 1999; Berube et al., 2005). To evaluate the outcome of *Atrx* loss of function on mitotic cells in vivo during corticogenesis, brain sections from four different *Atrx* null and littermate controls were fixed and stained with DAPI to visualize nuclei and chromatin and the status of mitotic neuroepithelial cells lining the ventricular space was evaluated. We observed a high occurrence of pyknotic nuclei, which is indicative of cells undergoing apoptosis in the vicinity of mitotic cells, which confirms previous findings (Berube et al., 2005). We also observed a very high incidence of micronuclei or misaligned chromosomes (Fig. 5 B). We quantified the occurrence of micronulei/misaligned chromosomes by scoring both hemispheres in sections from four littermate *Atrx* null and control embryos and limited our analysis to the mitotic layer that lines the hippocampal hem, the hippocampal primordium, and the dorsal cortical neuroepithelium (Fig. 5 C, between 1 and 2). This analysis revealed a significant increase in the number of micronulei in *Atrx* null mice compared with controls (Fig. 5 C), which suggests that *Atrx* loss of function in vivo in mouse neuroprogenitors causes mitotic defects that are similar to those observed by RNA interference in cultured human cells.

Discussion

It has been suggested that brain size is partly dictated by the correct expression of genes that control neuroprogenitor mitosis. Microcephalin (Alderton et al., 2006; Bartek, 2006), abnormal spindlelike microcephaly associated (Bond et al., 2002; Fish et al., 2006), Cdk 5 regulatory-associated protein 2, and CENP-J (Bond et al., 2005) all have roles in assembling, maintaining, and orienting the mitotic spindle and mutations of these genes in humans causes primary microcephaly. Our data now suggest that the loss of both ATRX protein isoforms (full-length and truncated forms), either by transient or stable depletion, in HeLa cells causes defective sister chromatid cohesion and chromosome congression at the metaphase plate and that loss of ATRX in the mouse forebrain also results in mitotic defects. Although ATRX is highly enriched at PCH, we did not detect abnormal targeting of CENP-E, CENP-F, or HP1α or in the enrichment of histone modifications that characterize condensed chromatin at PCH. However, we did observe a general effect on chromosome condensation in metaphasic chromosomes that will require further investigation. Misaligned chromosomes were also observed at meiosis II upon RNA interference of *Atrx* expression and by antibody injections in mouse oocytes (De La Fuente et al., 2004). It is unclear at present whether similar phenomena are responsible for the meiotic and mitotic defects, but it is possible that the loss of centromeric cohesion could explain misalignment of chromosomes at meiosis II. Further investigation of ATRX function on chromatin dynamics and architecture during meiosis will be required to clarify these issues.

Several genes involved in chromosome cohesion cause multiple developmental abnormalities when mutations arise in humans. The best examples to date include the *NIPBL* (delangin), *SMC1A*, and *SMC3* genes mutated in Cornelia de Lange syndrome (CdLS) and the *ESCO2* gene mutated in Robert's syndrome (Krantz et al., 2004; Vega et al., 2005; Musio et al., 2006; Borck et al., 2007; Deardorff et al., 2007). All of these factors are components of the cohesin complex or regulators of cohesin loading or unloading. Syndromes caused by *ATRX* mutations display partial phenotypic overlap with CdLS, including cognitive delay, craniofacial dysmorphisms, microcephaly, gastrointestinal defects, and problems with the genitourinary system, hearing, and ocular development. Another similarity between ATRX and NIPBL is a shared protein motif that confers the ability to associate with the HP1α CSD (Lechner et al., 2005).

ATRX now joins other chromatin remodeling complexes implicated in cohesion, such as RSC and Snf2h/NURD, either by loading cohesin during DNA replication or recruiting the cohesin complex to specific chromosomal regions (Hakimi et al., 2002; Baetz et al., 2004; Huang et al., 2004; Huang and Laurent, 2004). Although the cohesin complex is required for normal chromatid cohesion during mitosis, it also has a function in facilitating long-range enhancer–promoter interactions. The developmental abnormalities in CdLS and the ATRX syndromes could therefore be explained by the specific deregulation of gene expression at loci that rely on long-range enhancer interactions mediated by the cohesin complex and its regulators. An important focus of research will therefore be to identify such target genes and determine how chromosome cohesion might control their expression.

Materials and methods

Cell culture and transfection

HeLa (American Type Culture Collection) and HG cells (a gift from G.M. Wahl, Salk Institute for Biological Studies, La Jolla, CA) were grown at 37°C with 5% CO_2 in DME supplemented with 10% FBS (Sigma-Aldrich). HG growth media was supplemented with 2 μg/ml blasticidin S HCl (Invitrogen) to maintain transgene expression. For siRNA transfection, cells were seeded 24 h before transfection using Lipofectamine 2000 (Invitrogen) according to the manufacturer's instructions. The final siRNA concentration used in all experiments was 8 nM. In HeLa cells, the transfection efficiency was ∼90–95% based on immunofluorescence detection of the ATRX protein isoforms. For population synchronization at G1/S, transfected cells were incubated with 10 μM hydroxyurea and released after 16 h by removal of the drug.

RNA interference

The synthetic oligonucleotides siATRX1 (5′-GAGGAAACCUUCAAUUGUAUU-3′), siATRX2 (5′-GCAGAGAAAUUCCUAAAGAUU-3′), and siATRX1 scrambled (5′-GAUUGAAGACUGAUAUCACUU-3′) were obtained from Dharmacon. The control (nontargeting) duplex was obtained from Sigma-Aldrich. siRNA duplexes were transfected with Lipofectamine 2000 according to the manufacturer's instructions. Mock-transfected samples were treated similarly but without the addition of siRNA.

Western blot analysis

Cells were lysed with RIPA buffer (150 mM NaCl, 1% NP-40, 50 mM Tris, pH 8.0, 0.5% deoxycholic acid, 0.1% SDS, 0.2 mM PMSF, 0.5 mM NaF, 0.1 mM Na_3VO_4, and 1 protease inhibitor cocktail tablet [Complete mini, EDTA-free; Roche]) for 5 min on ice. Extracts were sonicated and quantified using the DC protein assay (Bio-Rad Laboratories). 20 μg of protein was resolved on 6 or 12% SDS-PAGE and transferred onto nitrocellulose membranes (Bio-Rad Laboratories). The membranes were probed with rabbit α-ATRX H300 (Santa Cruz Biotechnology, Inc.), mouse α-ATRX 39f (a gift of D.J. Picketts, Ottawa Health Research Institute, Ottawa, Canada; and D. Higgs, University of Oxford, Oxford, UK), followed by the appropriate horseradish peroxidase–conjugated secondary antibody (1:5,000; GE Healthcare). After washing, the membrane was incubated in ECL before exposure to x-ray film. The membrane was reprobed with mouse α–α-tubulin (1:40,000; Sigma-Aldrich) as a loading control.

Q-RT-PCR analysis

Total RNA was isolated using the RNeasy mini kit (QIAGEN). First-strand cDNA was synthesized from 3 μg of total RNA using random primers and a reverse transcription cocktail containing 5× first strand buffer, 100 mM DTT, 25 mM dNTPs, RNA guard (GE Healthcare), and Superscript RT (Invitrogen). PCR reactions were performed on a continuous fluorescence detector (Chromo4; MJ Research) in the presence of iQ SYBR green supermix (Bio-Rad Laboratories) and analyzed with Opticon Monitor 3 and GeneX software (Bio-Rad Laboratories) using the standard curve corresponding threshold method of quantification. Samples were amplified as follows: 95°C for 30 s, 55°C for 30 s, and 72°C for 30 s. After 30 cycles, a melting curve was generated to visualize amplicon purity. Standard curves were generated for each primer pair using fivefold serial dilutions of control cDNA. Primer efficiency was calculated as $\%E = [(10^{(-1/slope)}) - 1] \times 100\%$, where a desirable slope is –3.32 and $r^2 > 0.99$. All data were normalized GAPDH expression levels. The primers used for Q-RT-PCR were as follows: ATRX-F, 5′-TCCTTGCACACTCATCAGAAGAATC-3′; ATRX-R, 5′-CGTGACGATCCTGAAGACTTGG-3′; GAPDH-F, 5′-GAGTCAACGGATTTGGTCGT-3′; and GAPDH-R, 5′-GACAAGCTTCCCGTTCTCAG-3′.

Flow cytometry

Exponentially growing cells were harvested, washed with calcium/magnesium-free (CMF) PBS (137 mM NaCl, 2.7 mM KCl, 1.5 mM potassium phosphate monobasic, and 12 mM sodium phosphate dibasic) three times and 1.5×10^6 cells were fixed dropwise with 90% ethanol and stored at 4°C for at least 12 h. To detect DNA content, cells were washed and stained with propidium iodide/RNase staining solution (10 μg/ml propidium iodide), 250 μg/ml RNase A (Sigma-Aldrich), and 2% BSA in CMF PBS for 30 min at room temperature followed by overnight incubation at 4°C. Cell populations were analyzed by flow cytometry on an EPICS XL-MCL instrument (Beckman-Coulter). Data analysis to determine the proportion of cells in each phase of the cell cycle was performed using the Expo 32 software package (Beckman Coulter).

Indirect immunofluorescence microscopy

For immunofluorescence detection, cells were fixed with 3:1 ethanol/methanol up to 4 d after control or siRNA transfection and incubated with the following

primary antibodies: α-ATRX H300 (1:200; Santa Cruz Biotechnology, Inc.), α-ATRX 39f (1:20; provided by D.J. Picketts), α–α-tubulin (1:1,500; Sigma-Aldrich), α-phosphohistone H3(S10) (1:200; Millipore), human α-CREST (1:10,000; W. Brinkley, Baylor College of Medicine, Houston, TX), α-BubR1 (1:200; BD Biosciences), α-Bub1 (1:1,000; a gift from S. Taylor, University of Manchester, Manchester, UK), α-CENP-E (1:400; Santa Cruz Biotechnology, Inc.), α–CENP-F (a gift from S. Taylor), α-HP1α (1:200; Millipore), and α-HP1β (1:200; Millipore). Secondary antibodies included goat α–rabbit Alexa 594 (1:1,500), donkey α–rabbit Alexa 488 (1:1,500), goat α–mouse Alexa 488 (1:1,500), goat α–mouse Alexa 594 (1:1,500), and goat α–human Alexa 647 (1:1,500; Invitrogen). Coverslips were mounted with Vectashield H-1000 (Vector Laboratories).

Generation of ATRX-depleted stable clones

Pairs of sense 60-mer oligonucleotides corresponding to the 19-mer siATRX1 and siATRX2 siRNA target sequences and their reverse complement (underlined sequences) were designed that contained 5′ BglII and 3′ HindIII restriction sites to facilitate cloning (Integrated DNA Technologies, Inc.). Sequences were as follows: shATRX1 (sense), 5′-GATCCCCGAGGAAACCTTCAATTGTATTCAAGAGATACAATTGAAGGTTTCCTCTTTTTA-3′, and shATRX2 (sense), 5′GATCCCCGCAGAGAAATTCCTAAAGATTCAAGAGATCTTTAGGAATTTCTCTGCTTTTTA-3′. The oligonucleotides were annealed to complimentary antisense 60-mer oligonucleotides in buffer containing 10 mM Tris, pH 7.5, 50 mM NaCl, and 1 mM EDTA at 90°C for 4 min followed by 70°C for 10 min, and then step cooled to 37°C for 20 min using a thermocycler (MJ Research) and cloned into the pSuper.retro.neo plasmid (Oligoengine) using the Quick ligation kit according to manufacturer's instructions (New England Biolabs, Inc.). The resulting vectors, designated pSUPER-shATRX1 and pSUPER-shATRX2, were subsequently sequenced to confirm sequence identity. Exponentially growing HG were transfected with empty pSuper vector or with pSuper-shATRX1 and pSuper-shATRX2 vectors (1 μg/ml) using Lipofectamine 2000. 2 d after transfection, cells were replated at low density and selection was applied 24 h later (800 μg/ml geneticin; Invitrogen). Drug-resistant colonies were picked and expanded in selection media (400 μg/ml geneticin).

Time-lapse and live cell microscopy

HeLa-HG, HG-pSuper, HG-shATRX1, or HG-shATRX2 cells were plated on 35-mm glass-bottom tissue culture dishes (MatTek) in DME with 10% FBS. After 24 h, the media was replaced with CO_2-independent media (Invitrogen) supplemented with 10% FBS and 4 mM L-glutamine (Sigma-Aldrich). For transient experiments, cells were plated and transfected and scored 48–72 h after transfection. Cells were imaged using an automated inverted microscope (DMI 6000b; Leica) equipped with a live cell stage-mounted environment chamber (Neue Biosciences) to maintain the cells at 37°C during imaging. Phase-contrast and fluorescence (GFP) images were captured every 3 min for 10 h using Openlab Software automation (5.0; PerkinElmer). To measure mitotic duration, cells that initiated mitosis (determined by nuclear envelope breakdown) and reentered G1 (nuclear decondensation) within the time frame of the experiment (10 h) were analyzed ($n > 50$). This analysis did not include cells that were arrested at prometaphase or that died during the timeframe of the experiment. To measure the frequency of unaligned chromosomes at metaphase, cells were seeded in 35-mm culture wells (BD Biosciences) in DME with 10% FBS and at least 500 metaphase cells were scored per sample. For mitotic spindle checkpoint arrest, HeLa-HG or HG-shATRX1 cells were treated with 100 ng/ml nocodazole for 16 h. Rounded mitotic cells and adherent interphase cells were quantified using live cell microscopy ($n > 1{,}000$).

Fixed chromosome spreads

HeLa cells were transiently transfected with no siRNA duplex (mock), siATRX1 scrambled (nonspecific control), siATRX1, or siATRX2. 70 h after transfection, mitotically arrested cells were removed by shake-off and adherent cells were treated with 100 ng/ml KaryoMAX Colcemid (Invitrogen) for 2 h. Mitotic cells were then isolated and incubated in hypotonic solution (75 mM KCl) for 20 min followed by fixation in Carnoy's Fix (3:1 methanol/acetic acid) and stored at −20°C. Fixed cells were dropped onto Superfrost Plus glass microscope slides (Thermo Fisher Scientific) and air dried; DNA was counterstained with 100 ng/ml DAPI and mounted in Vectashield H-1000. For z-stack imaging, 0.4-μm-interval z stacks were captured and deconvolved using iterative restoration with Volocity imaging software (4.0; PerkinElmer).

Measure of interkinetochore distances

To measure interkinetochore distance, mitotic HeLa-HG, HG-pSuper, HG-shATRX1, and HG-shATRX2 stable cells were fixed in 3:1 ethanol/methanol and the kinetochores were stained using the human CREST antibody (1:10,000) and imaged using a 63× 1.4 NA oil immersion objective (Leica). Z stacks were captured at 0.4-μm z intervals spanning 20 μm. Kinetochore pairs were connected from the outer edges of the CREST signal and the distance was measured using Volocity software. Only kinetochore pairs in single optical sections that were aligned at the metaphase plate were used to measure interkinetochore distances ($n \geq 100$). Statistical differences were assessed by ANOVA. Significant differences in mean interkinetochore distance were assessed by ANOVA and a Tukey's multiple comparison post hoc test. Differences were considered significant when $P < 0.05$. Statistical analysis was performed using GraphPad Prism (4.02; GraphPad Software, Inc.).

Kinetochore microtubule assay

HeLa-HG, HG-pSuper, HG-shATRX1, or HG-shATRX2 cells were seeded in 35-mm dishes (Corning) in 2 ml DME with 10% FBS on 22-mm^2 glass coverslips (VWR). After 48 h, the growth medium was replaced with ice-cold growth medium and the cells were incubated on ice for 10 min. The cells were rinsed twice with ice-cold PHEM buffer (60 mM piperazine ethanesulfonic acid, 45 mM Hepes, 10 mM EGTA, and 2 mM $MgCl_2$, pH 6.9), permeabilized with cold 0.5% Triton X-100 in PHEM buffer for 3 min, and fixed in cold 3.5% paraformaldehyde in PHEM for 15 min. The coverslips were rinsed with PHEM and processed for immunofluorescence staining and microscopy.

Analysis of mitotic cells in the developing telencephalon

The generation of *Atrx*^{loxP} mice was described previously (obtained from D. Higgs and R. Gibbons, University of Oxford; Berube et al., 2005; Garrick et al., 2006). Male embryos conditionally deficient for Atrx were obtained by crossing homozygous *Atrx*^{loxP} females to heterozygous Foxg1Cre knock-in male mice and embryonic yolk sac DNA from E13.5 embryos was genotyped by PCR as described previously (Berube et al., 2005). Midday of the day of vaginal plug discovery was considered to be E0.5. At scheduled times, pregnant females were anesthetized with CO_2 and killed by cervical dislocation. Embryos and postnatal brains were fixed in 4% paraformaldehyde/PBS overnight at 4°C, sunk in 30% sucrose in PBS, and embedded in 15% sucrose and 50% optimal cutting temperature compound (Sakura). Tissue sections were cut at 10-μm thickness and mounted on SuperFrost Plus slides, air dried at room temperature, and stored at −80°C. For immunofluorescence staining, sections were thawed, rehydrated in PBS for 10 min, counterstained with DAPI, and mounted in Vectashield. Micronuclei and misaligned chromosomes from the mitotic layer lining the lateral ventricle were scored from both hemispheres of brain sections ($n = 3$) in four litter-matched control and ATRX null embryos using fluorescence microscopy. Analysis was restricted to the mitotic layer that lines the hippocampal hem, hippocampal primordium, and the dorsal cortical neuroepithelium (indicated by the area between 1 and 2 in Fig. 5 C).

Details of image acquisition and processing

All samples processed for microscopy were imaged using a DMI 6000b automated inverted microscope. IF images were captured using a 63× 1.4 NA oil immersion lens, a 40× 1.25 NA oil immersion lens (Leica), or a 5× dry objective (Leica). For oil immersion microscopy, we used immersion oil with a refractive index of 1.518 (Leica). All images were captured at ambient temperature except for image capture of live cells and time-lapse experiments, which were performed at 37°C. Experiments used different combinations of DAPI, goat anti–rabbit Alexa 594, goat anti–mouse Alexa 594, donkey anti–rabbit Alexa 488, goat anti–mouse Alexa 488, and goat anti–human 594 secondary antibodies. Digital microscopy images were captured with a digital camera (ORCA-ER; Hammamatsu). Openlab imaging software was used for manual and automated image capture and processing was performed using Volocity. All deconvolution was performed using iterative restoration set with a confidence limit of 95%.

Online supplemental material

Fig. S1 shows the validation of ATRX depletion in HeLa cells. Fig. S2 shows prolonged mitotic time in ATRX-depleted cells. Fig. S3 shows HP1α and HP1β staining in ATRX-depleted cells. Fig. S4 shows abnormal spindle morphology in ATRX-depleted cells. Online supplemental material is available at http://www.jcb.org/cgi/content/full/jcb.200706083/DC1.

We are grateful to Jamie Seabrook for help with statistical analysis, and Douglas Higgs and Richard Gibbons for the *Atrx*^{loxP} mice.

This work was supported by the Canadian Institutes for Health Research (CIHR; grant MOP-74748) and the Hospital for Sick Children Foundation (grant XG-05-012R) operating grants to N.G. Bérubé. N.G. Bérubé is a CIHR New Investigator.

Submitted: 12 June 2007
Accepted: 18 December 2007

References

Alderton, G.K., L. Galbiati, E. Griffith, K.H. Surinya, H. Neitzel, A.P. Jackson, P.A. Jeggo, and M. O'Driscoll. 2006. Regulation of mitotic entry by microcephalin and its overlap with ATR signalling. *Nat. Cell Biol.* 8:725–733.

Baetz, K.K., N.J. Krogan, A. Emili, J. Greenblatt, and P. Hieter. 2004. The ctf13-30/CTF13 genomic haploinsufficiency modifier screen identifies the yeast chromatin remodeling complex RSC, which is required for the establishment of sister chromatid cohesion. *Mol. Cell. Biol.* 24:1232–1244.

Bartek, J. 2006. Microcephalin guards against small brains, genetic instability, and cancer. *Cancer Cell.* 10:91–93.

Berube, N.G., C.A. Smeenk, and D.J. Picketts. 2000. Cell cycle-dependant phosphorylation of the ATRX protein correlates with changes in nuclear matrix and chromatin association. *Hum. Mol. Genet.* 9:539–547.

Berube, N.G., M. Mangelsdorf, M. Jagla, J. Vanderluit, D. Garrick, R.J. Gibbons, D.R. Higgs, R.S. Slack, and D.J. Picketts. 2005. The chromatin-remodelling protein ATRX is critical for neuronal survival during corticogenesis. *J. Clin. Invest.* 115:258–267.

Berube, N.G., J. Healy, C.F. Medina, S. Wu, T. Hodgson, M. Jagla, and D.J. Picketts. 2007. Patient mutations alter ATRX targeting to PML nuclear bodies. *Eur. J. Hum. Genet.* In press.

Bond, J., E. Roberts, G.H. Mochida, D.J. Hampshire, S. Scott, J.M. Askham, K. Springell, M. Mahadevan, Y.J. Crow, A.F. Markham, et al. 2002. ASPM is a major determinant of cerebral cortical size. *Nat. Genet.* 32:316–320.

Bond, J., E. Roberts, K. Springell, S.B. Lizarraga, S. Scott, J. Higgins, D.J. Hampshire, E.E. Morrison, G.F. Leal, E.O. Silva, et al. 2005. A centrosomal mechanism involving CDK5RAP2 and CENPJ controls brain size. *Nat. Genet.* 37:353–355.

Borck, G., M. Zarhrate, J.P. Bonnefont, A. Munnich, V. Cormier-Daire, and L. Colleaux. 2007. Incidence and clinical features of X-linked Cornelia de Lange syndrome due to SMC1L1 mutations. *Hum. Mutat.* 28:205–206.

Ciosk, R., M. Shirayama, A. Shevchenko, T. Tanaka, A. Toth, and K. Nasmyth. 2000. Cohesin's binding to chromosomes depends on a separate complex consisting of Scc2 and Scc4 proteins. *Mol. Cell.* 5:243–254.

De La Fuente, R., M.M. Viveiros, K. Wigglesworth, and J.J. Eppig. 2004. ATRX, a member of the SNF2 family of helicase/ATPases, is required for chromosome alignment and meiotic spindle organization in metaphase II stage mouse oocytes. *Dev. Biol.* 272:1–14.

Deardorff, M.A., M. Kaur, D. Yaeger, A. Rampuria, S. Korolev, J. Pie, C. Gil-Rodriguez, M. Arnedo, B. Loeys, A.D. Kline, et al. 2007. Mutations in cohesin complex members SMC3 and SMC1A cause a mild variant of cornelia de Lange syndrome with predominant mental retardation. *Am. J. Hum. Genet.* 80:485–494.

Fish, J.L., Y. Kosodo, W. Enard, S. Paabo, and W.B. Huttner. 2006. Aspm specifically maintains symmetric proliferative divisions of neuroepithelial cells. *Proc. Natl. Acad. Sci. USA.* 103:10438–10443.

Gandhi, R., P.J. Gillespie, and T. Hirano. 2006. Human Wapl is a cohesin-binding protein that promotes sister-chromatid resolution in mitotic prophase. *Curr. Biol.* 16:2406–2417.

Garrick, D., V. Samara, T.L. McDowell, A.J. Smith, L. Dobbie, D.R. Higgs, and R.J. Gibbons. 2004. A conserved truncated isoform of the ATR-X syndrome protein lacking the SWI/SNF-homology domain. *Gene.* 326:23–34.

Garrick, D., J.A. Sharpe, R. Arkell, L. Dobbie, A.J.H. Smith, W.G. Wood, D.R. Higgs, and R.J. Gibbons. 2006. Loss of Atrx affects trophoblast development and the pattern of X-inactivation in extraembryonic tissues. *PLoS Genetics.* 2:e58.

Gibbons, R.J., D.J. Picketts, L. Villard, and D.R. Higgs. 1995. Mutations in a putative global transcriptional regulator cause X-linked mental retardation with alpha-thalassaemia (ATR-X syndrome). *Cell.* 80:837–845.

Hakimi, M.A., D.A. Bochar, J.A. Schmiesing, Y. Dong, O.G. Barak, D.W. Speicher, K. Yokomori, and R. Shiekhattar. 2002. A chromatin remodelling complex that loads cohesin onto human chromosomes. *Nature.* 418:994–998.

Hirano, T. 2005. SMC proteins and chromosome mechanics: from bacteria to humans. *Philos. Trans. R. Soc. Lond. B Biol. Sci.* 360:507–514.

Hoffelder, D.R., L. Luo, N.A. Burke, S.C. Watkins, S.M. Gollin, and W.S. Saunders. 2004. Resolution of anaphase bridges in cancer cells. *Chromosoma.* 112:389–397.

Huang, J., and B.C. Laurent. 2004. A Role for the RSC chromatin remodeler in regulating cohesion of sister chromatid arms. *Cell Cycle.* 3:973–975.

Huang, J., J.M. Hsu, and B.C. Laurent. 2004. The RSC nucleosome-remodeling complex is required for Cohesin's association with chromosome arms. *Mol. Cell.* 13:739–750.

Kitajima, T.S., T. Sakuno, K. Ishiguro, S. Iemura, T. Natsume, S.A. Kawashima, and Y. Watanabe. 2006. Shugoshin collaborates with protein phosphatase 2A to protect cohesin. *Nature.* 441:46–52.

Krantz, I.D., J. McCallum, C. DeScipio, M. Kaur, L.A. Gillis, D. Yaeger, L. Jukofsky, N. Wasserman, A. Bottani, C.A. Morris, et al. 2004. Cornelia de Lange syndrome is caused by mutations in NIPBL, the human homolog of *Drosophila melanogaster* Nipped-B. *Nat. Genet.* 36:631–635.

Kueng, S., B. Hegemann, B.H. Peters, J.J. Lipp, A. Schleiffer, K. Mechtler, and J.M. Peters. 2006. Wapl controls the dynamic association of cohesin with chromatin. *Cell.* 127:955–967.

Lechner, M.S., D.C. Schultz, D. Negorev, G.G. Maul, and F.J. Rauscher III. 2005. The mammalian heterochromatin protein 1 binds diverse nuclear proteins through a common motif that targets the chromoshadow domain. *Biochem. Biophys. Res. Commun.* 331:929–937.

McDowell, T.L., R.J. Gibbons, H. Sutherland, D.M. O'Rourke, W.A. Bickmore, A. Pombo, H. Turley, K. Gatter, D.J. Picketts, V.J. Buckle, et al. 1999. Localization of a putative transcriptional regulator (ATRX) at pericentric heterochromatin and the short arms of acrocentric chromosomes. *Proc. Natl. Acad. Sci. USA.* 96:13983–13988.

McEwen, B.F., G.K. Chan, B. Zubrowski, M.S. Savoian, M.T. Sauer, and T.J. Yen. 2001. CENP-E is essential for reliable bioriented spindle attachment, but chromosome alignment can be achieved via redundant mechanisms in mammalian cells. *Mol. Biol. Cell.* 12:2776–2789.

McGuinness, B.E., T. Hirota, N.R. Kudo, J.M. Peters, and K. Nasmyth. 2005. Shugoshin prevents dissociation of cohesin from centromeres during mitosis in vertebrate cells. *PLoS Biol.* 3:e86.

Melcher, M., M. Schmid, L. Aagaard, P. Selenko, G. Laible, and T. Jenuwein. 2000. Structure-function analysis of SUV39H1 reveals a dominant role in heterochromatin organization, chromosome segregation, and mitotic progression. *Mol. Cell. Biol.* 20:3728–3741.

Musio, A., A. Selicorni, M.L. Focarelli, C. Gervasini, D. Milani, S. Russo, P. Vezzoni, and L. Larizza. 2006. X-linked Cornelia de Lange syndrome owing to SMC1L1 mutations. *Nat. Genet.* 38:528–530.

Peters, A.H., D. O'Carroll, H. Scherthan, K. Mechtler, S. Sauer, C. Schofer, K. Weipoltshammer, M. Pagani, M. Lachner, A. Kohlmaier, et al. 2001. Loss of the Suv39h histone methyltransferases impairs mammalian heterochromatin and genome stability. *Cell.* 107:323–337.

Picketts, D.J., D.R. Higgs, S. Bachoo, D.J. Blake, O.W.J. Quarrell, and R.J. Gibbons. 1996. *ATRX* encodes a novel member of the SNF2 family of proteins: mutations point to a common mechanism underlying ATR-X syndrome. *Hum. Mol. Genet.* 5:1899–1907.

Sumara, I., E. Vorlaufer, P.T. Stukenberg, O. Kelm, N. Redemann, E.A. Nigg, and J.M. Peters. 2002. The dissociation of cohesin from chromosomes in prophase is regulated by Polo-like kinase. *Mol. Cell.* 9:515–525.

Takata, H., S. Matsunaga, A. Morimoto, N. Ma, D. Kurihara, R. Ono-Maniwa, M. Nakagawa, T. Azuma, S. Uchiyama, and K. Fukui. 2007. PHB2 protects sister-chromatid cohesion in mitosis. *Curr. Biol.* 17:1356–1361.

Tanudji, M., J. Shoemaker, L. L'Italien, L. Russell, G. Chin, and X.M. Schebye. 2004. Gene silencing of CENP-E by small interfering RNA in HeLa cells leads to missegregation of chromosomes after a mitotic delay. *Mol. Biol. Cell.* 15:3771–3781.

Vega, H., Q. Waisfisz, M. Gordillo, N. Sakai, I. Yanagihara, M. Yamada, D. van Gosliga, H. Kayserili, C. Xu, K. Ozono, et al. 2005. Roberts syndrome is caused by mutations in ESCO2, a human homolog of yeast ECO1 that is essential for the establishment of sister chromatid cohesion. *Nat. Genet.* 37:468–470.

Watrin, E., A. Schleiffer, K. Tanaka, F. Eisenhaber, K. Nasmyth, and J.M. Peters. 2006. Human Scc4 is required for cohesin binding to chromatin, sister-chromatid cohesion, and mitotic progression. *Curr. Biol.* 16:863–874.

Wood, K.W., R. Sakowicz, L.S. Goldstein, and D.W. Cleveland. 1997. CENP-E is a plus end-directed kinetochore motor required for metaphase chromosome alignment. *Cell.* 91:357–366.

Xue, Y., R. Gibbons, Z. Yan, D. Yang, T.L. McDowell, S. Sechi, J. Qin, S. Zhou, D. Higgs, and W. Wang. 2003. The ATRX syndrome protein forms a chromatin-remodeling complex with Daxx and localizes in promyelocytic leukemia nuclear bodies. *Proc. Natl. Acad. Sci. USA.* 100:10635–10640.

Yang, Z., J. Guo, Q. Chen, C. Ding, J. Du, and X. Zhu. 2005. Silencing mitosin induces misaligned chromosomes, premature chromosome decondensation before anaphase onset, and mitotic cell death. *Mol. Cell. Biol.* 25:4062–4074.

Yao, X., K.L. Anderson, and D.W. Cleveland. 1997. The microtubule-dependent motor centromere-associated protein E (CENP-E) is an integral component of kinetochore corona fibers that link centromeres to spindle microtubules. *J. Cell Biol.* 139:435–447.